Available online at www.sciencedirect.com
ScienceDirect
Journal of the European Ceramic Society 28 (2008) 2681–2686
www.elsevier.com/locate/jeurceramsoc

Crystallographic texture in Al_2O_3–ZrO_2 (Y_2O_3) directionally solidified eutectics

J. Ramírez-Rico [a,*], A.R. de Arellano-López [a], J. Martínez-Fernández [a], J.I. Peña [b], A. Larrea [b]

[a] *Departamento de Física de la Materia Condensada-ICMSE, Universidad de Sevilla-CSIC, P.O. Box 1065, 41080 Sevilla, Spain*
[b] *Instituto de Ciencia de Materiales de Aragón, CSIC-Universidad de Zaragoza, E-50.018 Zaragoza, Spain*

Received 21 February 2008; received in revised form 22 April 2008; accepted 23 April 2008
Available online 9 June 2008

Abstract

Directionally solidified Al_2O_3-based eutectics are in situ composites grown from the melt. The directional nature of the solidification process makes these materials highly anisotropic and therefore the measurement and quantification of their crystallographic texture is necessary to understand their physical properties. We studied the texture of Al_2O_3–ZrO_2 (12 mol% Y_2O_3) eutectic rods by means of X-ray and electron backscattering diffraction. The phases grow according to the relationship $\{1\,0\,\bar{1}\,2\}_{Al_2O_3}//\{1\,1\,0\}_{ZrO_2}$ and Al_2O_3 is oriented with its *c*-axis approximately parallel to the growth direction. We observed that the *c*-axis orientation is not constant throughout the sample, but instead changes according to the distance from the growth axis. The *c*-axis orientation spread was found to be 10°. This spread is a consequence of the curvature of the liquid–solid interface during solidification, whose shape we reconstructed using EBSD data.

Keywords: Al_2O_3; ZrO_2; Electron microscopy; X-ray methods; Eutectics

1. Introduction

Directionally solidified Al_2O_3-based oxide eutectics have been the subject of great interest lately[1] due to their excellent mechanical strength, creep resistance and enhanced fracture toughness, as compared to their sintered counterparts. These properties have been attributed to the eutectic microstructure, which ranges from fibrous to lamellar depending on composition and growth conditions. Additionally, directionally solidified (DS) oxide eutectics are highly textured, due to the high thermal gradients applied, and usually have well-defined orientation relationships between the constituent phases. This texture makes directionally solidified eutectics highly anisotropic.

It has been shown that the mechanical performance of directionally solidified oxide eutectics is very sensitive to texture and microstructure, which can vary with different growth conditions. For example flexure strength varies with the characteristic microstructural length in DS Al_2O_3-YSZ rods.[2] Further refinement in the microstructure accompanied by a good texture in Al_2O_3–$Y_3Al_5O_{12}$-YSZ DSE yields the exceptional bending strength of 4.6 GPa.[3] In addition, dislocations have been shown to play an important role in the creep behaviour of Al_2O_3–$Y_3Al_5O_{12}$.[4] Since Al_2O_3 slip is highly anisotropic, its crystallographic orientation in the eutectic will greatly affect its plasticity. For these reasons, a comprehensive understanding of the texture is important in order to predict the mechanical response in these materials.

The crystallographic texture of Al_2O_3–ZrO_2 with different amounts of Y_2O_3 has been studied in directionally solidified rods and plates in the past, mostly using X-rays or electron diffraction in the TEM.[5–8] In the case of X-ray diffraction, preferred orientation was determined by comparison of the diffractograms acquired at several orientations of the eutectics in Bragg-Brentano geometry with those obtained from the powder precursors. Only Starostin et al. studied the texture of Al_2O_3–ZrO_2 by means of pole figure analysis.[9] In the case of TEM, crystallographic orientation relationships between phases were determined, but no attempt to determine spatial variations of texture was made, mainly due to the difficulty of carrying out such studies in TEM. Only in the case of the ZrO_2–$CaZrO_3$ DS eutectic the misorientation between adjacent lamellae in a regular zone formed by ~60 alternating lamellae (~70 μm width and

* Corresponding author.
E-mail address: jrr@us.es (J. Ramírez-Rico).

0955-2219/$ – see front matter © 2008 Elsevier Ltd. All rights reserved.
doi:10.1016/j.jeurceramsoc.2008.04.015

more than 1 mm long) has been studied using Kikuchi electron diffraction patterns in the TEM.[10] Unfortunately this technique is not appropriate for extended areas due to the huge amount of work and to the impossibility of preparing electron transparent areas of the whole sample. In contrast, the electron backscattered diffraction (EBSD) technique has proved very useful for the study of directionally solidified materials,[11,12] since it can be used to correlate texture and microstructure up to millimeter length scales. For example, Frazer et al.[11] used conventional X-ray pole figure analysis to determine the macroscopic texture of directionally solidified Al_2O_3–$Y_3Al_5O_{12}$, and determined spatial variations in crystallographic orientation using EBSD.

In this paper we study the crystallographic orientation of Al_2O_3–ZrO_2 (12% Y_2O_3) directionally solidified eutectics grown by the laser float zone method (LFZ), by means of X-ray diffraction and EBSD. We use these complementary techniques to determine the orientation relationships between the two phases and to measure the spatial variations of the texture.

2. Experimental

2.1. Eutectic solidification

Rods of Al_2O_3–ZrO_2 (12% Y_2O_3) eutectic were grown using a technique previously described elsewhere.[7] In brief, precursors were prepared using a mixture of commercial powders of ZrO_2, Y_2O_3 and Al_2O_3 at the eutectic composition 62.0 mol% Al_2O_3, 33.4 mol% ZrO_2 and 4.6 mol% Y_2O_3. At this composition the ZrO_2 phase is expected to be fully stabilized in the cubic form. Powders were milled, fired in air at 1000 °C for 0.5 h, hand milled in an agate mortar and mixed. Precursor rods were prepared by isostatic pressing for 2 min at 200 MPa. The rods thus obtained were sintered in a furnace at 1500 °C for 12 h and then directionally solidified with the LFZ method using a CO_2 laser at a growth rate of 1000 mm/h. Rods with diameters of around 2 mm were obtained.

2.2. SEM and EBSD measurements

SEM samples were prepared using conventional metallographic techniques, which involved grinding and polishing with diamond paste down to 0.25 μm. Samples for standard SEM observations were coated with carbon. For EBSD measurements, an additional ion milling step was performed as described previously.[11] No conductive coating was applied in the samples observed in EBSD. Electron energy was 25 keV, and the samples were tilted at 70° with respect to beam direction. The observations were carried out using a TSL Digiview (EDAX) camera in a Philips XL-30 conventional SEM. The data analysis was performed using TSL OIM Analysis v3.5 software.

The EBSD technique has been described elsewhere.[13–19] In brief, the electron beam of a SEM is diffracted by the sample surface when tilted adequately. The resulting diffraction pattern is called a Kikuchi pattern and can be recorded in a phosphor screen using a digital camera and indexed using a computer program to calculate the orientation of the sample volume that is interacting with the beam. By using the scanning capabilities of a SEM, thousands of equidistant points in the sample surface can be measured automatically, generating orientation maps in which crystallographic data is spatially resolved. Since the spatial resolution of the EBSD apparatus used here was not enough to resolve the microstructural features present in the material, it was not possible to obtain detailed orientation maps. Instead, line scans were acquired to determine the spatial variations of the texture, at a step size that was too big to resolve the microstructure but small enough to resolve variations across a transverse section of the sample. Indexed diffraction patterns with a confidence index[16] lower than 0.2 were discarded.

2.3. X-ray diffraction measurements

X-ray texture measurements were performed using an X-ray single crystal diffractometer (Bruker D8 Smart Apex) equipped with a CCD area detector. A pinhole collimator of 0.5 mm in diameter was used. Sections perpendicular to the growth direction were polished and studied in reflection using Mo-K radiation. Diffraction patterns were acquired at different orientations by rotating the sample in 5 degree steps in a kappa goniometer. Experimental setup and angular coverage have been previously described.[20] The resulting images were then analyzed and the XRD2D software[20,21] was used for extracting pole figures. The orientation distribution function was calculated by the WIMV algorithm using the popLA software[22] and additional non-measured pole figures were reconstructed by projection of the resulting orientation distribution function.[15,16]

3. Results and discussion

3.1. Microstructure

SEM images of Al_2O_3–ZrO_2 (12% Y_2O_3) are shown in Fig. 1 for sections perpendicular to the growth direction, and are similar to those reported previously.[7] The microstructure is formed of cells elongated along the growth direction, composed of finely dispersed ZrO_2 fibers embedded in an Al_2O_3 matrix. The colonies are surrounded by a coarser intercolonial area composed of both Al_2O_3 and ZrO_2 phases.

3.2. X-ray diffraction

Fig. 2 shows a representative X-ray diffractogram acquired using Mo-K radiation in reflection. The presence of incomplete circles is evidence of the texture present in the material. The rings corresponding to $\{1\,0\,\bar{1}\,2\}$ and $\{2\,0\,\bar{2}\,4\}$ Al_2O_3 and $\{1\,1\,0\}$ cubic ZrO_2 reflections are marked. It can be guessed from the figure that those planes are parallel in the eutectic, as will become evident after the pole figure analysis. By measuring the diffracted intensity variations along each circle, for different sample orientations, pole figures can be measured for all diffracting planes.

Some reconstructed pole figures are displayed in Fig. 3a. It is evident that the following relationships apply:

$$\{1\,0\,\bar{1}\,2\}_{Al_2O_3}//\{1\,1\,0\}_{ZrO_2}$$

$$[0\,0\,0\,1]_{Al_2O_3}//\langle 1\,1\,0\rangle_{ZrO_2}//\text{Growth Direction}$$

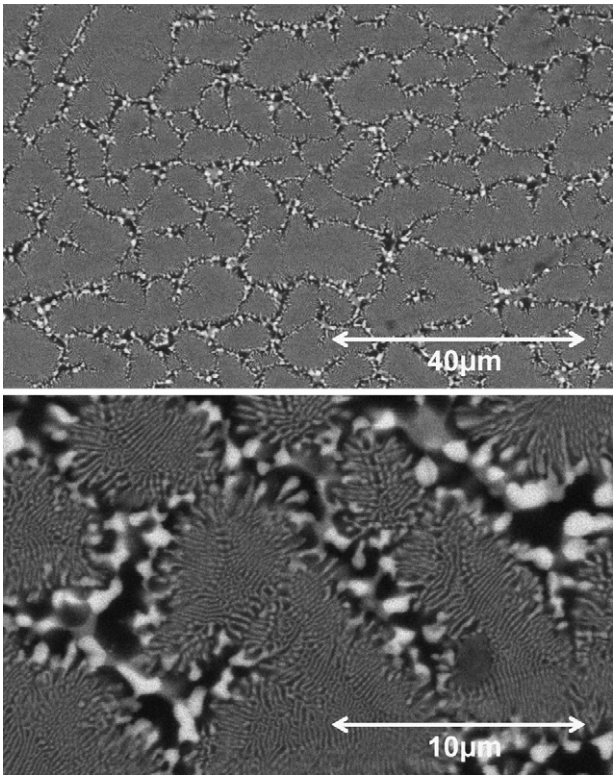

Fig. 1. SEM micrographs of transverse sections of Al_2O_3–ZrO_2 (12% Y_2O_3).

where $[0\,0\,0\,1]_{Al_2O_3}$ and $\langle 1\,1\,0\rangle_{ZrO_2}$ are the growth directions as they are parallel to the rod axis. These results agree with those previously reported for samples grown using the LFZ method at rates up to 300 mm/h,[7,23] and also for samples grown using the Stepanov technique.[9]

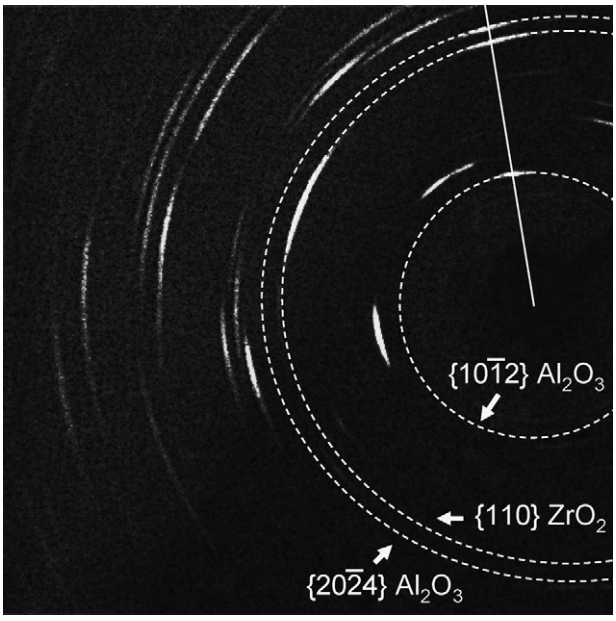

Fig. 2. Representative X-ray diffractogram acquired using Mo-K radiation in reflection. The presence of incomplete circles is evidence of the texture present in the material. The alignment of the $\{1\,0\,\bar{1}\,2\}$ reflection in Al_2O_3 and the $\{1\,1\,0\}$ reflection of cubic ZrO_2 is shown by a white line.

3.3. EBSD

Clear EBSD patterns could be acquired for both Al_2O_3 and ZrO_2 phases, although a fair proportion were a superposition of patterns from both constituents. No significant charging was observed. Two representative diffraction patterns are shown in Fig. 4. It is clear that their quality was good enough for indexing purposes.

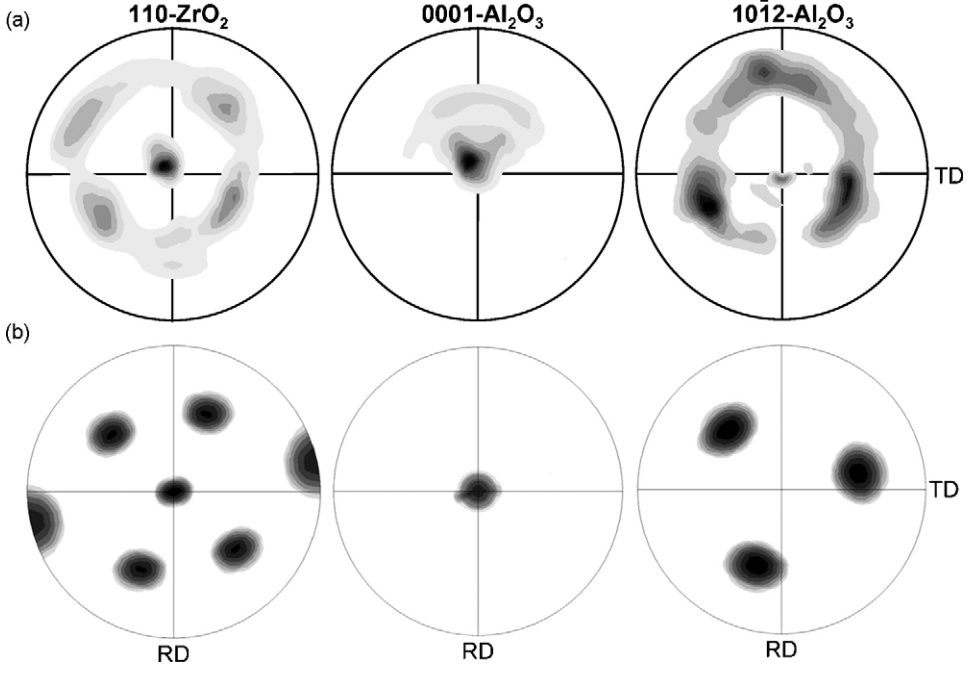

Fig. 3. (a) Reconstructed pole figures, calculated using the WIMV algorithm from the experimental pole figures measured by X-ray diffraction. Scale is linear, arbitrary units. (b) Experimental pole figures obtained from a 10 μm × 10 μm area by discrete binning in EBSD.

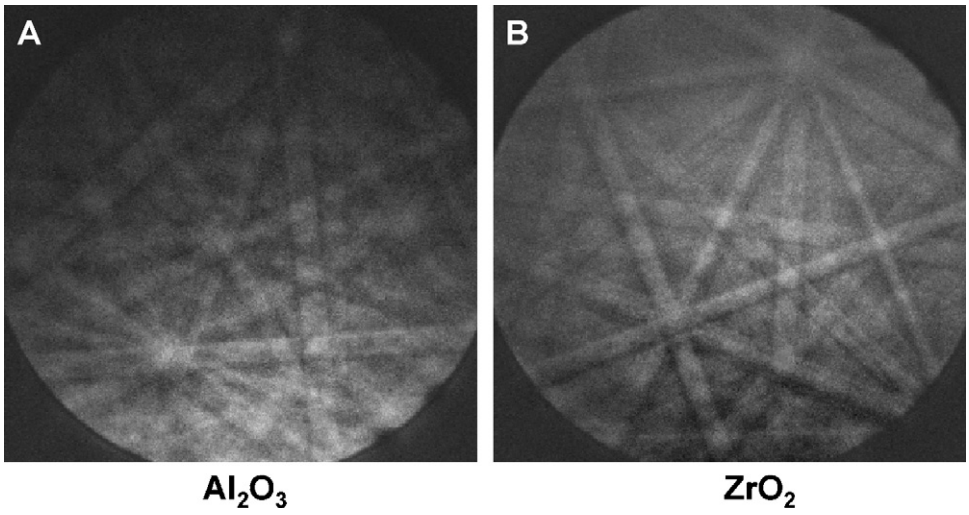

Fig. 4. EBSD diffraction patterns from Al_2O_3 (A) and ZrO_2 (B). No charging effects were observed and the quality of the patterns was good enough for indexing.

Pole figures calculated from EBSD data acquired from a 10 μm × 10 μm area are shown in Fig. 3b for comparison with the reconstructed XRD data. This area was chosen as it is about the average colony area in the eutectic microstructure. Unfortunately, our spatial resolution was not enough to resolve the different phases, and for that reason no orientation map is presented. However, after discarding the likely misindexed points, pole figures matching the overall orientation measured by XRD could be calculated. The texture obtained by EBSD is sharper, as it corresponds to a smaller area of the sample.

To determine the spatial variations of the texture perpendicular to the growth diameter, an EBSD line scan along a full diameter of the eutectic rod was performed, at 1 μm steps. Clearly, this step size is not enough to resolve the microstructural features observed in SEM, but since it is smaller than the average colony size, it is enough to determine orientation variations in adjacent colonies. Discrete pole figures of (0 0 0 1) and {1 0 $\bar{1}$ 2} reflections of Al_2O_3 are shown in Fig. 5, where the transverse direction (TD) is parallel to the scanned diameter of the rod. In the figure, the discrete orientations have different shades of grey, according to the distance from the axis of the eutectic rod. It can be seen that, although the *c*-axis of Al_2O_3 is approximately parallel to the growth direction, its orientation varies along the diameter of the rod. This variation gives rise to the broadening of the pole figure maxima along the horizontal direction (TD) in both (0 0 0 1) and {1 0 $\bar{1}$ 2} pole figures. The *c*-axis orientation spread of Al_2O_3 was found to be 10°, measured as the full width at half maximum of the intensity distribution of the (0 0 0 1) pole figure along the scanned diameter. This effect was also observed in the ZrO_2 phase, but since it is present in the eutectic in only 30% volume, the pole figures calculated with ZrO_2 show much less detail and we have chosen to omit them.

The spatial variation of orientation can be explained if we assume that during the eutectic solidification the Al_2O_3 phase grows with its *c*-axis perpendicular to the liquid–solid interface. Since the oxide melt strongly absorbs the 10.6 μm CO_2 radiation, a radial temperature gradient is established, making the liquid–solid interface convex towards the melt. This was observed by de Francisco et al.[24] who studied the shape of the solidification front as a function of growth parameters. By suddenly turning the laser off during eutectic growth, they were able to freeze the melt and reveal the solid–liquid interface, which could then be observed by SEM in sections parallel to the growth direction.

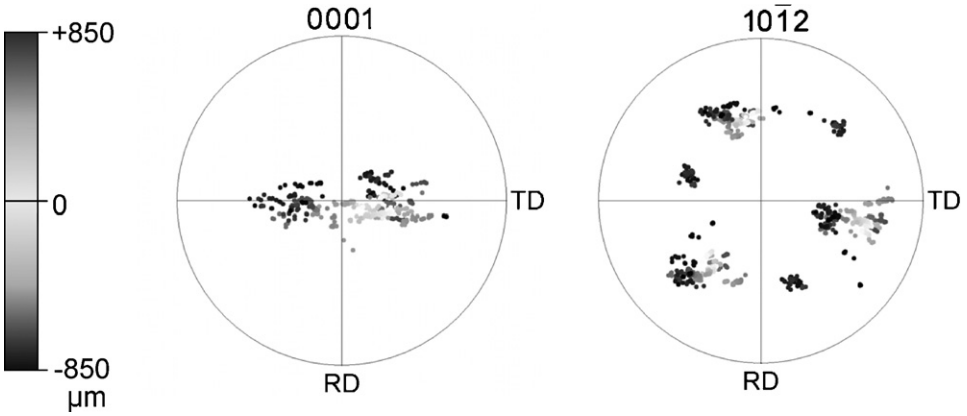

Fig. 5. Discrete pole figures from EBSD measurements. Data was acquired along a full diameter of a transverse section, parallel to TD. The discrete points are shaded according to their distance from the centre of the rod. In the (0 0 0 1) pole figure the polar angle is represented up to 30°.

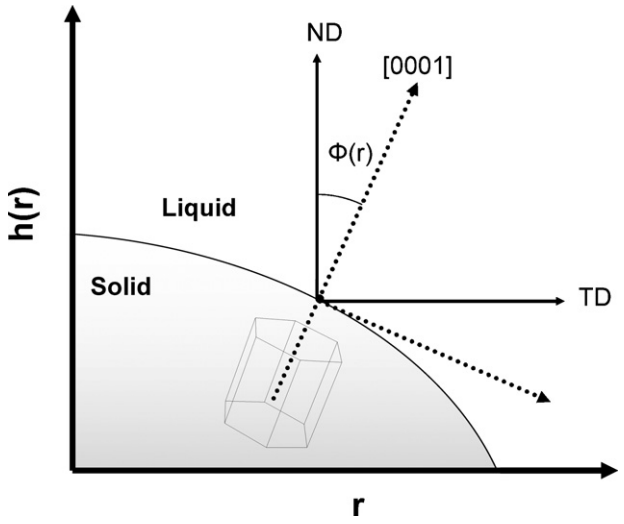

Fig. 6. Relationship between the shape of the liquid–solid interface and the angle between the growth direction and [0 0 0 1] direction in Al_2O_3, assuming that it is perpendicular to the liquid–solid interface.

We will describe the shape of the liquid–solid interface as a function $h(r)$ that gives the height of the solidification front as a function of the distance from the growth axis r, as depicted in Fig. 6. If we assume that the Al_2O_3 phase is oriented with its c-axis perpendicular to the interface, then Φ is the angle formed by the c-axis and the growth axis and is simply given by (see Fig. 6):

$$\tan\Phi(r) = \frac{\mathrm{d}h(r)}{\mathrm{d}r} \tag{1}$$

Since the function $\Phi(r)$ is directly measured by EBSD, we can obtain the shape of the solid–liquid interface by numerical integration of Eq. (1), i.e.

$$h(r) = \int_0^r \tan\Phi(r')\,\mathrm{d}r' + C \tag{2}$$

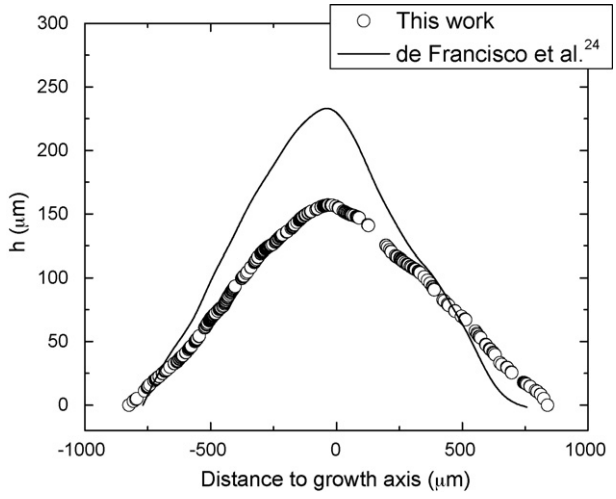

Fig. 7. Shape of the liquid–solid interface during solidification, reconstructed from the orientation data shown in Fig. 4. Data from de Francisco et al.[24] is included for comparison. See text for details.

where C is simply an integration constant. We present the calculated shape of the solid–liquid interface in Fig. 7, where data from Ref.[24] is included for comparison. It can be seen that the agreement is reasonable, thus confirming our hypothesis that the variations in crystallographic orientation observed are a consequence of the curvature of the solidification front. The measurements included in Fig. 7 from Ref.[24] were made on eutectics with 3 mol% Y_2O_3 grown at 10 mm/h, thus the solidification front profiles cannot be directly compared. In fact our measured profile is significantly flatter than that measured by de Francisco et al. because of the higher growth rate (1000 mm/h) used in our case.

4. Conclusions

We have successfully studied the macroscopic texture of Al_2O_3–ZrO_2 (12% Y_2O_3) eutectics grown by the laser heated float zone technique at 1000 mm/h, by analysis of pole figures obtained by X-ray diffraction. We have also studied the material using EBSD to discover spatial variations in the macroscopic texture. Our analysis shows that the phases grow according to the relationship $[0\,0\,0\,1]_{Al_2O_3}//\langle 1\,1\,0\rangle_{ZrO_2}$ approximately parallel to the growth direction. Due to the curvature of the solid–liquid interface, the tilt angle between the $[0\,0\,0\,1]_{Al_2O_3}$ and the growth directions increases with the distance from the rod axis. By measuring this tilt angle along a diameter of a transverse section of the rod and assuming that the c-axis of Al_2O_3 grows perpendicular to the solid–liquid interface, we have been able to reconstruct the shape of the solidification front.

Acknowledgements

This work was supported by the Spanish Ministry of Science and Technology through Grant MAT 2006-13005-C03-01. The authors are grateful to the CITIUS at the University of Seville for the use of their electron microscopy facilities and to the CIC at the University of Granada for the use of their X-ray diffraction facilities. We are grateful to Dr. Rodríguez-Navarro for his help acquiring XRD data. J.R.-R. is grateful to the Junta de Andalucía for his pre-doctoral grant.

References

1. Llorca, J. and Orera, V. M., Directionally solidified eutectic ceramic oxides. *Prog. Mater. Sci.*, 2006, **51**, 711–809.
2. Pastor, J. Y., Llorca, J., Poza, P., de Francisco, I., Merino, R. I. and Peña, J. I., Mechanical properties of melt-grown Al_2O_3–ZrO_2 (Y_2O_3) eutectics with different microstructure. *J. Eur. Ceram. Soc.*, 2005, **25**, 1215–1223.
3. Oliete, P. B., Peña, J. I., Larrea, A., Orera, V. M., LLorca, J., Pastor, J. Y. *et al.*, Ultra-high-strength nanofibrillar Al_2O_3–YAG-YSZ eutectics. *Adv. Mater.*, 2007, **19**, 2313–2318.
4. Ramirez-Rico, J., Pinto-Gomez, A. R., Martinez-Fernandez, J., de Arellano-Lopez, A. R., Oliete, P. B., Peña, J. I. *et al.*, High-temperature plastic behaviour of Al_2O_3–$Y_3Al_5O_{12}$ directionally solidified eutectics. *Acta Mater.*, 2006, **54**, 3107–3116.
5. Mazerolles, L., Michel, D. and Hÿtch, M. J., Microstructures and interfaces in directionally solidified oxide-oxide eutectics. *J. Eur. Ceram. Soc.*, 2005, **25**, 1389–1395.

6. Mazerolles, L., Michel, D. and Portier, R., Interfaces in oriented Al_2O_3–ZrO_2 (Y_2O_3) eutectics. *J. Am. Ceram. Soc.*, 1986, **69**, 252–255.
7. Peña, J. I., Merino, R. I., Harlan, N. R., Larrea, A., de la Fuente, G. F. and Orera, V. M., Microstructure of Y_2O_3 doped Al_2O_3–ZrO_2 eutectics grown by the laser floating zone method. *J. Eur. Ceram. Soc.*, 2002, **22**, 2595–2602.
8. Larrea, A., de la Fuente, G. F., Merino, R. I. and Orera, V. M., ZrO_2–Al_2O_3 eutectic plates produced by laser zone melting. *J. Eur. Ceram. Soc.*, 2002, **22**, 191–198.
9. Starostin, M. Y., Gnesin, B. A. and Yalovets, T. N., Microstructure and crystallographic phase textures of the alumina-zirconia eutectics. *J. Cryst. Growth*, 1997, **171**, 119–124.
10. Larrea, A., Orera, V. M., Peña, J. I. and Merino, R. I., Orientation relationship and interfaces in nonfaceted-nonfaceted ZrO_2 (c)-$CaZrO_3$ lamellar eutectics. *J. Mater. Res.*, 1999, **14**, 2588–2593.
11. Frazer, C. S., Dickey, E. C. and Sayir, A., Crystallographic texture and orientation variants in Al_2O_3–$Y_3Al_5O_{12}$ directionally solidified eutectic crystals. *J. Cryst. Growth*, 2001, **233**, 187–195.
12. López-Robledo, M. J., Ramírez-Rico, J., Martínez-Fernández, J., de Arellano-López, A. R. and Sayir, A., Microestructura y comportamiento plástico de perovsquitas conductoras protónicas de alta temperatura. *Bol. Soc. Esp. Ceram. V.*, 2005, **44**, 347.
13. Coates, D. G., Kikuchi-Like Reflection Patterns Obtained with Scanning Electron Microscope. *Philos. Mag.*, 1967, **16**, 1179–1184.
14. Dingley, D. J., In *The Development of Automated Diffraction in Scanning and Transmission Microscopy, in Electron Backscatter Diffraction in Materials Science*, ed. A. J. Schwartz, M. Kumar and B. L. Adams. Plenum, New York, 2000.
15. Kocks, U. F., Tomé, C. N. and Wenk, H.-R., *Texture and Anisotropy*. Cambridge University Press, Cambridge, 1998.
16. Randle, V. and Engler, O., *Introduction to Texture Analysis*. CRC Press, New York, 2000.
17. Venables, J. A. and Binjaya, R., Accurate micro-crystallography using electron backscattering patterns. *Philos. Mag.*, 1977, **35**, 1317–1332.
18. Wright, S. I. and Adams, B. L., Automated lattice orientation determination from electron backscatter kikuchi diffraction patterns. *Texture. Microstruct.*, 1991, **14**, 273–278.
19. Wright, S. I. and Adams, B. L., Automatic-analysis of electron backscatter diffraction patterns. *Metall. Mater. Trans. A*, 1992, **23**, 759–767.
20. Rodriguez-Navarro, A. B., Registering pole figures using an X-ray single-crystal diffractometer equipped with an area detector. *J. Appl. Crystallogr.*, 2007, **40**, 631–634.
21. Rodriguez-Navarro, A. B., XRD2DScan: new software for polycrystalline materials characterization using two-dimensional X-ray diffraction. *J. Appl. Crystallogr.*, 2006, **39**, 905–909.
22. Kallend, J. S., Kocks, U. F., Rollett, A. D. and Wenk, H. R., Popla—an integrated software system for texture analysis. *Texture. Microstruct.*, 1991, **14**, 1203–1208.
23. Sayir, A. and Farmer, S. C., The effect of the microstructure on mechanical properties of directionally solidified Al_2O_3/ZrO_2 (Y_2O_3) eutectic. *Acta Mater.*, 2000, **48**, 4691–4697.
24. de Francisco, I., Merino, R. I., Orera, V. M., Larrea, A. and Peña, J. I., Growth of Al_2O_3/ZrO_2 (Y_2O_3) eutectic rods by the laser floating zone technique: effect of the rotation. *J. Eur. Ceram. Soc.*, 2005, **25**, 1341–1350.